# Reconfigurable Holographic Surface-aided Distributed MIMO Radar Systems

Qian Li, Graduate Student Member, IEEE, Ziang Yang, Graduate Student Member, IEEE, Dou Li, Hongliang Zhang, Member, IEEE

Abstract—Distributed phased Multiple-Input Multiple-Output (phased-MIMO) radar systems have attracted wide attention in target detection and tracking. However, the phase-shifting circuits in phased subarrays contribute to high power consumption and hardware cost. To address this issue, an energy-efficient and cost-efficient metamaterial antenna array, i.e., reconfigurable holographic surface (RHS), has been developed. In this letter, we propose RHS-aided distributed MIMO radar systems to achieve more accurate multi-target detection under equivalent power consumption and hardware cost as that of distributed phased-MIMO radar systems. Different from phased arrays, the RHS achieves beam steering by regulating the radiation amplitude of its elements, and thus conventional beamforming schemes designed for phased arrays are inapplicable. Aiming to maximize detection accuracy, we design an amplitude-controlled beamforming scheme for multiple RHS subarrays. The simulations validate the superiority of the proposed scheme over the distributed phased-MIMO radar scheme and reveal the optimal allocation between coherent processing gain and diversity gain for optimal system performance with fixed hardware resources.

Index Terms—Distributed radar systems, reconfigurable holographic surface, semi-positive programming.

#### I. Introduction

ISTRIBUTED multiple-input multiple-output (MIMO) radar [1] consists of widely separated antennas that can observe targets from different angles, thus reducing the scintillation of the radar cross section (RCS). By transmitting orthogonal waveforms, it can separate all the transceiver paths and achieve spatial diversity gain, thereby enhancing the performance of target detection but losing the coherence array-processing gain of traditional phased array radar.

In order to combine the spatial diversity gain of distributed MIMO radar and the coherent processing gain of phased array radar, distributed phased-MIMO radar [2] is proposed, which replaces each antenna in distributed MIMO radar with a phased subarray. However, due to the power-consuming and high-cost hardware circuits composed of phase shifters and power amplifiers in distributed phased-MIMO radar, the aperture of the system is limited, making it difficult to improve performance.

A new type of metasurface antenna array [3], [4] called reconfigurable holographic surface (RHS) [5] is developed to address the above issues. The RHS contains a large number of metamaterial elements, and the beam is regulated by controlling the radiation amplitude of each RHS element.

The authors are with the School of Electronics, Peking University, Beijing, China (e-mail: qianli@stu.pku.edu.cn; {yangziang,lidou,hongliang.zhang}@pku.edu.cn).

Specifically, the RHS regulates the beam with simple diodes, which are much more power-efficient and cost-effective than phase shifters and power amplifiers in phased arrays. The power consumption is defined as the total power consumed by the antenna, including the radiation power and the power consumed by the hardware circuits. According to the RHS prototype [6], the ratio of radiation power to total power of RHS and phased array is approximated as  $\eta_R=25\%$  and  $\eta_A=4\%$ , respectively. On average, the hardware cost of a phased array antenna is  $\delta=6\sim10$  [6] times that of an RHS element. Therefore, subjected to the same power consumption and cost as the phased array, the RHS can achieve a larger array aperture, so that the detection accuracy can be improved. In addition, some studies [7], [8] have investigated the impact of hardware impairments in the design of RHS beamforming.

In literature, there are some works [9], [10] that investigate RHS radar system to achieve target detection. In [9], the authors proposed an RHS-enabled holographic radar and derived the globally optimal closed-form RHS beamformer with the highest signal-to-noise ratio (SNR). In [10], the authors proposed an RHS based radar system and designed a joint waveform and amplitude optimization algorithm for multitarget detection. However, they are based on single-static RHS radar system, and there is a lack of research on RHS-aided distributed MIMO radar systems, which need to design the beamformer of multiple subsystems jointly making the design of such a scheme more complicated.

In this letter, we investigate RHS-aided distributed MIMO radar systems for multi-target detection. Nevertheless, the design of the beamforming scheme presents following challenges. First, the multi-target/clutter multi-subsystem architecture increases the complexity of system performance evaluation. Second, the RHS achieves beamforming through regulating the radiation amplitude of its elements, which means conventional phase-shifting schemes are inapplicable. To address these challenges, firstly, we formulate an optimization problem aiming to maximize multi-target detection capability while balancing the performance of all subsystems. Secondly, we develop an amplitude optimization algorithm that jointly optimizes beamformers of all RHS subarrays. In the simulation, we compare the proposed scheme with the distributed phased-MIMO radar scheme under equal power consumption and hardware cost, and verify the advantages of the proposed scheme. Additionally, to enhance performance, we simulate the spatial diversity gain and coherent processing gain obtained by increasing hardware resources, and explore the optimal allocation of these gains when hardware resources are fixed.

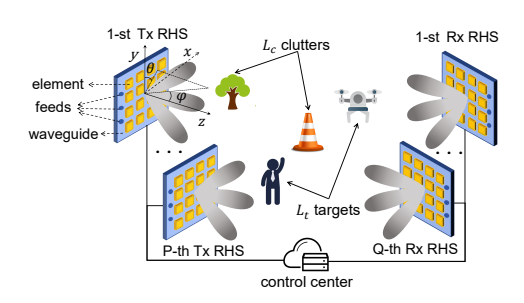


Fig. 1. System model for RHS-aided distributed MIMO radar.

#### II. SYSTEM MODEL

In this section, we model RHS-aided distributed radar systems at first, and then introduce the RHS model and the signal model of the proposed system.

## A. Scenario Description

As shown in Fig. 1, RHS-aided distributed MIMO radar systems consist of P Tx RHS subarrays, Q Rx RHS subarrays,  $L_t$  static targets,  $L_c$  clutters and a control center. Each Tx/Rx RHS contains  $N_t = N_r = N_x \times N_y$  elements and  $K_t = K_r = K$  feeds, and all subarrays are randomly distributed in space. The total number of elements in the system, i.e. hardware resources of the system [2], is  $N_{sum} = PN_t + QN_r$ . The reflection coefficient of each target/clutter is inhomogeneous, and each target/clutter is in a different direction from each subarray. The control center of the system is connected to the subarrays, processing the received signals and controlling the beams of the subarrays to improve system performance.

# B. RHS model

The RHS is a type of leaky wave metamaterial antenna, which consists of three parts: K feeds, a waveguide, and numerous densely arranged sub-wavelength metamaterial elements [5]. The feeds convert injected signals into electromagnetic waves, i.e., reference waves. The RHS adopts series feeding, where the reference wave propagates in the waveguide and excites the RHS elements one by one, and then leaks out from each element independently into free space. The RHS achieves amplitude-controlled holographic beamforming based on the principle of holographic interference. The radiated amplitude  $\psi$  of each RHS element is mapped by the real part of the interference,  $Re\left[\Psi_{intf}\right]$  (i.e., the cosine value of the phase difference between the reference wave and the object wave). And to avoid negative values,  $Re\left[\Psi_{intf}\right]$  is normalized to [0,1], i.e.,  $\psi = \left(Re\left[\Psi_{intf}\right] + 1\right)/2$ . In practical hardware, RHS elements with controllable radiation amplitude can be fabricated by loading varactor diodes and liquid crystals [11].

Assume that P Tx RHS subarrays respectively transmit P mutually orthogonal narrowband signal waveforms. In the p-th Tx RHS, it is assumed that the signal  $s_p \in \mathbb{C}^{1 \times I_t}$  is injected into all  $K_t$  feeds, where  $I_t$  denotes the number of snapshots. Thus the signal  $S_p \in \mathbb{C}^{K_t \times I_t}$  injected into the p-th Tx RHS consists of a stack of  $K_t$  vectors  $s_p$ . The signal  $X_p \in \mathbb{C}^{N_t \times I_t}$  radiated by the p-th Tx RHS can be expressed as:

$$\boldsymbol{X}_{p} = \boldsymbol{\varPsi}_{p}^{t} \left( \boldsymbol{Q}_{p}^{t} \circ \boldsymbol{\varGamma}_{p}^{t} \right) \boldsymbol{S}_{p}, \tag{1}$$

where  $\boldsymbol{\Psi}_p^t = diag\left\{\boldsymbol{\psi}_p^t\right\}$ , with  $\boldsymbol{\psi}_p^t = \left[\boldsymbol{\psi}_{p,1}^t,...,\boldsymbol{\psi}_{p,N_t}^t\right]$  as the beamformer of the p-th TX RHS, which is realized by a simple diode circuit controlling the radiation amplitude of each element in the RHS. The matrices  $\boldsymbol{Q}_p^t \in \mathbb{C}^{N_t \times K_t}$  and  $\boldsymbol{\Gamma}_p^t \in \mathbb{C}^{N_t \times K_t}$  respectively indicate the inherent phase shift and amplitude attenuation matrices when the reference signal propagates in the RHS waveguide. The symbol  $\circ$  denotes the Hadamard product. The  $(n_t,k_t)$ -th element of  $\boldsymbol{Q}_p^t$  can be given by  $q_{n_t,k_t}^t = e^{-j2\pi\nu D_{n_t,k_t}/\lambda}$ , where  $D_{n_t,k_t}$  represents the distance between the  $k_t$ -th feed and the  $n_t$ -th element,  $\lambda$  is the wavelength of the signal,  $\nu$  is the refractive index. The  $(n_t,k_t)$ -th element of  $\boldsymbol{\Gamma}_p^t$  can be given by  $\gamma_{n_t,k_t}^t = e^{-aD_{n_t,k_t}}$ , where a is the amplitude attenuation factor.

Due to the reciprocity of antennas, the signal received by the q-th Rx RHS subarray can be expressed as:

$$Y_q = \left[ \Psi_q^r \left( Q_q^r \circ \Gamma_q^r \right) \right]^T V, \tag{2}$$

where  $\pmb{V} \in \mathbb{C}^{N_r \times I_r}$  denotes the echo signal with  $I_r$  being the number of snapshots,  $\pmb{\varPsi}_q^r = diag\left\{\pmb{\psi}_q^r\right\}$ , with  $\pmb{\psi}_q^r = \left[\pmb{\psi}_{q,1}^r,...,\pmb{\psi}_{q,N_r}^r\right]$  as the beamforming vector of the q-th Rx RHS subarray. The matrices  $\pmb{Q}_q^r \in \mathbb{C}^{N_r \times K_r}$  and  $\pmb{\Gamma}_q^r \in \mathbb{C}^{N_r \times K_r}$  denotes the inherent phase shift and amplitude attenuation matrices of the Rx RHS, respectively, as defined for the Tx RHS.

## C. Received Signal Model

Suppose that P Tx RHS subarrays radiate signals, which propagate to  $L=L_t+L_c$  targets/clutters and reflect to Q Rx RHS subarrays. The signal at each Rx RHS is filtered through a matched filter bank  $S_p^{MF}, p=1,2,...,P$  where  $S_p^{MF}$  denotes the matched filter related to the p-th transmit signal. Due to the orthogonality of the transmitted signal,  $\sum_{i=1}^{I_t} s(i) s^H(i) = I_P$ , where  $s(i) = [s_1(i), ..., s_P(i)]^T \in \mathbb{C}^{P \times 1}$ , the output signal of the p-th matched filter of the q-th Rx RHS subarray, i.e.,  $\mathbf{Y}_{pq}$ , can be expressed as:

$$\mathbf{Y}_{pq} = \left[ \mathbf{\Psi}_q^r \left( \mathbf{Q}_q^r \circ \mathbf{\Gamma}_q^r \right) \right]^T \mathbf{V}_{pq}, \tag{3}$$

where

$$V_{pq} = \sum_{l=1}^{L} \left( \beta_{pq}^{l} \boldsymbol{A}_{pq}^{l} \boldsymbol{X}_{p} \boldsymbol{J}_{pq}^{l} \right) + \boldsymbol{N}_{pq}, \tag{4}$$

where  $\beta_{pq}^l$  is the reflection coefficient of the l-th target/clutter relative to the (p,q)-th transceiver array pair, and it is modeled as a Gaussian random variable with zero mean and variance  $\sigma_{pq}^{l}$  [6].  $A_{pq}^{l} = a_{q}^{l} \left(\vartheta_{q}^{l}, \varphi_{q}^{l}\right) \left(a_{p}^{l} \left(\vartheta_{p}^{l}, \varphi_{p}^{l}\right)\right)^{T}$ ,  $a_{q}^{l} \left(\vartheta_{q}^{l}, \varphi_{q}^{l}\right) \in \mathbb{C}^{N_{r} \times 1}$  and  $a_{p}^{l} \left(\vartheta_{p}^{l}, \varphi_{p}^{l}\right) \in \mathbb{C}^{N_{t} \times 1}$  respectively denote the steering vector of the l-th target/clutter with respect to the q-th Rx RHS and the p-th Tx RHS.  $\vartheta_{q}^{l}, \vartheta_{p}^{l}, \varphi_{p}^{l}, \varphi_{p}^{l}$  are the corresponding azimuth and elevation angles, respectively.  $J_{pq}^{l}$  is a shift matrix of size  $I_{t} \times I_{r}$ , representing the signal delay [12].  $N_{pq} \in \mathbb{C}^{N_{r} \times I_{r}}$  represents the matrix of the complex Gaussian noise of the (p,q)-th transceiver array pair after the corresponding matched filter, and the noise of the signal received by the q-th Rx RHS has mean 0 and variance  $\sigma_{n,q}^{2} =: \sigma_{n}^{2}$ .

## III. PROBLEM FORMULATION

Given the false alarm probability, the target detection probability increases monotonically with signal-to-interference-plusnoise-ratio (SINR) under Gaussian noise conditions [12], and thus we use SINR as the research index to evaluate the performance of target detection in this paper. Considering clutters and other targets as interferences, the SINR of the echo signal reflected by the  $l_t$ -th target by the (p,q)-th transceiver array pair can be expressed as:

$$SINR_{pq}^{l_{t}}\left(\boldsymbol{\psi}_{p}^{t},\boldsymbol{\psi}_{q}^{r}\right) = \frac{\left|\boldsymbol{v}_{pq}^{l_{t}}(\boldsymbol{\psi}_{p}^{t},\boldsymbol{\psi}_{q}^{r})\right|^{2}}{\sum\limits_{l=1,l\neq l_{t}}^{L}\left|\boldsymbol{v}_{pq}^{l}(\boldsymbol{\psi}_{p}^{t},\boldsymbol{\psi}_{q}^{r})\right|^{2} + \left|\boldsymbol{w}_{pq}\right|^{2}}, (5)$$

where  $v_{pq}^{l}(\boldsymbol{\psi}_{p}^{t}, \boldsymbol{\psi}_{q}^{r}) = \beta_{pq}^{l}vec\left[\left(\boldsymbol{\varPsi}_{q}^{r}\left(\boldsymbol{Q}_{q}^{r} \circ \boldsymbol{\Gamma}_{q}^{r}\right)\right)^{T}\boldsymbol{A}_{pq}^{l}\boldsymbol{X}_{p}\boldsymbol{J}_{pq}^{l}\right]$ and the noise term  $\boldsymbol{w}_{pq} = vec\left[\left(\boldsymbol{\varPsi}_{q}^{r}\left(\boldsymbol{Q}_{q}^{r}\circ\boldsymbol{\Gamma}_{q}^{r}\right)\right)^{T}\boldsymbol{N}_{pq}\right].$  In order to balance the performance of all subsystems, for

each target  $l_t$ , we can calculate  $\overline{SINR}^{l_t}$ , which is the average of the output SINR of all radar subsystems as

$$\overline{SINR}^{l_t} \left( \boldsymbol{\psi}^t, \boldsymbol{\psi}^r \right) = \sum_{p=1}^P \sum_{q=1}^Q \frac{1}{PQ} SINR_{pq}^{l_t} \left( \boldsymbol{\psi}_p^t, \boldsymbol{\psi}_q^r \right), \quad (6)$$

where  $\boldsymbol{\psi}^t = \left[\boldsymbol{\psi}_1^t,...,\boldsymbol{\psi}_P^t\right]^T \in \mathbb{R}^{\mathrm{PN}_t \times 1}$  with  $\boldsymbol{\psi}_p^t = \left(\boldsymbol{X}_p^t \boldsymbol{\psi}^t\right)^T$ , and the shift matrix  $\boldsymbol{X}_p^t$  as a block matrix where the p-th block matrix is  $I_{N_t}$  and the others are  $\mathbf{0}_{N_t}$ . Similarly, we denote  $\boldsymbol{\psi}^r = \begin{bmatrix} \boldsymbol{\psi}_1^r, ..., \boldsymbol{\psi}_Q^r \end{bmatrix}^T$  with  $\boldsymbol{\psi}_q^r = \begin{pmatrix} \boldsymbol{X}_q^r \boldsymbol{\psi}^r \end{pmatrix}^T$ . Under the multi-target scenario, the problem is designed to

maximize the worst case  $\overline{SINR}^{t_t}$  [12], and thus the max-min target detection optimization problem can be formulated as

P1: 
$$\max_{\boldsymbol{\psi}^{t}, \boldsymbol{\psi}^{r}} \min_{l_{t}} \left\{ \overline{SINR}^{l_{t}} \left( \boldsymbol{\psi}^{t}, \boldsymbol{\psi}^{r} \right) \right\},$$
 (7a)

s.t. 
$$tr\left\{ \left(\boldsymbol{\psi}^{t}\right)^{H}\boldsymbol{C}_{p}\boldsymbol{\psi}^{t}\right\} \leq P_{M}, \ \forall p,$$
 (7b)

$$0 \le \psi_{p,n_t}^t \le 1, \ \forall p, \forall n_t, \tag{7c}$$

$$0 \le \psi_{q,n_r}^r \le 1, \ \forall q, \forall n_r, \tag{7d}$$

where (7b) indicates that the radiation power of each Tx RHS does not exceed the upper bound  $P_{M}$ . The matrix  $C_{p} = \left(\boldsymbol{X}_{p}^{t}\right)^{H} \left[\left(\left(\boldsymbol{Q}_{p}^{t} \circ \boldsymbol{\Gamma}_{p}^{t}\right) \boldsymbol{S}_{p}\right) \left(\left(\boldsymbol{Q}_{p}^{t} \circ \boldsymbol{\Gamma}_{p}^{t}\right) \boldsymbol{S}_{p}\right)^{H}\right] \circ \boldsymbol{I}_{N_{t}} \boldsymbol{X}_{p}^{t}$ is Hermitian positive semidefinite, so (7b) is a quadratic convex constraint. Constraints (7c) and (7d) represent the magnitude constraints of each RHS element, which are linearly convex. The intersection of all constraints in (P1) is not empty, so that (P1) is feasible.

In the optimization objective of optimization problem P1,  $\psi^t$  and  $\psi^r$  are coupled together, which is difficult to solve directly, so we decouple problem (P1) into two sub-problems and solve them iteratively.

First, given beamformers for all Rx subarrays, namely  $\psi^r$ , optimize beamformers for all Tx subarrays, namely  $\psi^t$ .

$$P2: \max_{\boldsymbol{\psi}^{t}} \min_{l_{t}} \left\{ \overline{SINR}^{l_{t}} \left( \boldsymbol{\psi}^{t} \right) \right\}, \quad \text{s.t. } (7b), (7c). \quad (8)$$

Second, given the beamformers of all Tx subarrays, i.e.  $\psi^t$ , optimize the beamformers of all Rx subarrays, i.e.  $\psi^r$ .

$$P3: \max_{\boldsymbol{\psi}^r} \min_{l} \left\{ \overline{SINR}^{l_t} \left( \boldsymbol{\psi}^r \right) \right\}, \text{ s.t. } (7d).$$
 (9)

**Algorithm 1** Distributed RHS Radar Amplitude Optimization Algorithm (DRAOA)

**Input:** Initialize  $\Psi^{t(0)} = \mathbf{0}_{N_t+1}$ , randomly initialize  $\Psi^{r(0)}$ ; **Output:**  $\psi^t$ ,  $\psi^r$  and the objective function value  $\overline{SINR}^{l_t}$ ;

- 1: Set m = 1;
- 2: repeat
- Given  $\Psi^{r(m-1)}$ , solve (P2) to get  $\Psi^{t(m)}$  and  $U^{t(m)}$ ; Given  $\Psi^{t(m)}$ , solve (P3) to get  $\Psi^{r(m)}$  and  $U^{r(m)}$ ;
- Set m = m + 1;
- 6: **until**  $\left| U^{r(m)} U^{t(m)} \right| \le \epsilon$ ;
  7: Randomly generate  $\boldsymbol{\zeta}_g^t \sim N\left(0, \boldsymbol{\Psi}^t\right), \ g = 1, 2, ..., \ G$ , and  $\boldsymbol{\zeta}_h^r \sim N\left(0, \boldsymbol{\Psi}^r\right), \ h = 1, 2, ..., H$ .
- 8: Replace the out-of-range elements in  $\zeta_g^t$  and  $\zeta_h^r$  to satisfy (7c) and (7d) and delete  $\zeta_g^t$  that does not satisfy (7b).
- 9: select  $\zeta_g^t$  and  $\zeta_h^r$  that maximize the smallest  $\overline{SINR}^{l_t}$  as  $\psi^t$  and  $\psi^r$ , respectively.

#### IV. ALGORITHM DESIGN

In this section, we propose a distributed RHS radar amplitude optimization algorithm (DRAOA) as summarized in Algorithm 1, which solves problem (P1) by iteratively solving (P2) and (P3). The algorithms for solving subproblems (P2) and (P3) are described in the following sections.

## A. Transmit Amplitude Optimization

In this subsection, we aim to optimize the transmitting beamformer  $\psi^t$  given the receiving beamformer  $\psi^r$ . Since (P2) is a max-min fractional sum problem, this is a nonconvex NP-hard optimization problem. To facilitate the solu-

tion, firstly, we use positive semi-definite programming (SDP) [13]. Define  $\Psi^t = \begin{bmatrix} \psi^t \\ t \end{bmatrix} \begin{bmatrix} \psi^t \\ t \end{bmatrix}^H$ , where t is a variable t to homogenize SDP problem with  $t^2 = 1$ . Secondly, according to slack variable replacement (SVR) [12], we introduce two replacement variables  $U^t = \min_{l_t} \left\{ \overline{SINR}^{l_t} \left( \mathbf{\varPsi}^t \right) \right\}$  and  $\Lambda = \left\{\lambda_{pq}^{l_t}\right\}_{p=1,q=1,l_t=1}^{P,Q,L_t}$ , with  $\lambda_{pq}^{l_t} = SINR_{pq}^{l_t}\left(\boldsymbol{\Psi}^t\right)$ . After relaxing the rank-one constraint of  $\boldsymbol{\Psi}^t$ , we express (P2) as

$$P4: \max_{\boldsymbol{\Psi}^t \ U^t \ \boldsymbol{\Lambda}} \ U^t, \tag{10a}$$

s.t. 
$$Tr\left(\boldsymbol{C}_{p}^{'}\boldsymbol{\Psi}^{t}\right) \leq P_{M}, \ \forall p,$$
 (10b)

$$0 \le Tr\left(\boldsymbol{X}_{p,n_t}\,\boldsymbol{\varPsi}^t\right) \le 1, \ \forall p,n_t, \tag{10c}$$

$$\boldsymbol{\varPsi}^t \succ 0, \tag{10d}$$

$$Tr\left(\boldsymbol{D}^{t}\,\boldsymbol{\Psi}^{t}\right) = 1. \tag{10e}$$

$$\sum_{p=1}^{P} \sum_{q=1}^{Q} \frac{1}{PQ} \lambda_{pq}^{l_t} \ge U^t, \forall l_t, \tag{10f}$$

$$Tr\left[\left(\boldsymbol{R}_{pq}^{l_t'}-\lambda_{pq}^{l_t}\boldsymbol{R}_{pq}^{I'}\right)\boldsymbol{\varPsi}^{t}\right] \geq \lambda_{pq}^{l_t}$$
$$Tr\left(\boldsymbol{R}_{pq}^{N'}\boldsymbol{\varPsi}^{r}\right), \forall p, \ \forall q, \ \forall l_t.$$
 (10g)

where  $R_{pq}^{l_t'}$ ,  $R_{pq}^{I'}$ , and  $R_{pq}^{N'}$  represent the matrix  $R_{pq}^{l_t}$ ,  $R_{pq}^{I}$ , and  $R_{pq}^{N}$  expanded by one row and one column of zeros,

respectively, and  $\boldsymbol{R}_{pq}^{l_t} = \sum_{i_r=1}^{I_r} \left[ \left( \boldsymbol{H}_{pq}^{l_t} \boldsymbol{X}_p^t \right)^H \left( \boldsymbol{H}_{pq}^{l_t} \boldsymbol{X}_p^t \right) \right]$  with  $\boldsymbol{H}_{pq}^{l_t} = \beta_{pq}^{l_t} \left( \boldsymbol{\Psi}_q^r \left( \boldsymbol{Q}_q^r \circ \boldsymbol{\Gamma}_q^r \right) \right)^T \boldsymbol{A}_{pq}^{l_t} diag \left( \boldsymbol{Q}_p^t \circ \boldsymbol{\Gamma}_p^t \boldsymbol{S}_p \boldsymbol{J}_{pq}^{l_t} (i_r) \right)$ ,  $\boldsymbol{R}_{pq}^{I} = \sum_{l=1, l \neq l_t}^{L_t} \boldsymbol{R}_{pq}^{l_t}$ ,  $\boldsymbol{R}_{pq}^{N} = \sum_{i_r=1}^{I_r} \left( \boldsymbol{H}_{pq}^N \boldsymbol{X}_q^r \right)^H \left( \boldsymbol{H}_{pq}^N \boldsymbol{X}_q^r \right)$  with  $\boldsymbol{H}_{pq}^{N} = \left( \boldsymbol{Q}_q^r \circ \boldsymbol{\Gamma}_q^r \right)^T diag \left( \boldsymbol{N}_{pq} (i_r) \right)$ . Constraint (10b) corresponds to the radiation power constraint (7b), with  $\boldsymbol{C}_p'$  representing the matrix  $\boldsymbol{C}_p$  expanded by one row and one column of zeros. Constraint (10c) corresponds to (7c), which is a magnitude constraint, with  $\boldsymbol{X}_{p,n_t} = \begin{bmatrix} \boldsymbol{0}_{PN_t} & \boldsymbol{x}_{p,n_t} \\ (\boldsymbol{x}_{p,n_t})^T & 0 \end{bmatrix}$ , where  $\boldsymbol{x}_{p,n_t} \in \mathbb{R}^{PN_t \times 1}$ , which represents a column vector whose  $[(p-1) N_t + n_t]$ -th element is 1/2 and the remaining elements are 0. Constraint (10e) represents  $t^2 = 1$ , where  $\boldsymbol{D}^t$  is a square matrix of dimensions  $PN_t + 1$  with all zeros except for the last element, which is 1.

At this point, we can decompose the solution process of optimization problem (P4) into three simple steps, and solve them iteratively in sequence until convergence.

Firstly, solve problem (P5) using CVX. When  $U^{t(k-1)}$  and  $\boldsymbol{\Lambda}^{(k-1)}$  are given, the objective and constraints in subproblem (P5) are both convex, and can be easily solved.

$$P5: \max_{\Psi^t} \ U^t, \quad \text{s.t. } (10b)(10c)(10d)(10e)(10g).$$
 (11)

Secondly, calculate  ${\pmb \Lambda}^{(k)}$  using  ${\pmb \Psi}^{t\,(k)}$  in first step as

$$\lambda_{pq}^{l_t(k)} = \frac{Tr\left(\mathbf{R}_{pq}^{l_t'}\mathbf{\Psi}^{t(k)}\right)}{Tr\left(\mathbf{R}_{pq}^{I'}\mathbf{\Psi}^{t(k)}\right) + Tr\left(\mathbf{R}_{pq}^{N'}\mathbf{\Psi}^{r}\right)}.$$
 (12)

Thirdly, calculate  $U^{t(k)}$ . According to  $\Lambda^{t(k)}$  calculated in the second step, we can directly solve sub-problem (P6)

$$P6: \max_{U^t} \ U^t, \quad \text{s.t. } (10f).$$
 (13)

## B. Receive Amplitude Optimization

Similar to solving the transmit amplitude optimization subproblem (P2), firstly, we simplify the problem by using semidefinite relaxation (SDR) difining  $\boldsymbol{\Psi}^r = \begin{bmatrix} \boldsymbol{\psi}^r \\ s \end{bmatrix} \begin{bmatrix} \boldsymbol{\psi}^r \\ s \end{bmatrix}^H$ , with  $s^2 = 1$ . Secondly, we introduce two replacement variables:  $U^r = \min_{l_t} \left\{ \overline{SINR}^{l_t} \left( \boldsymbol{\Psi}^r \right) \right\}, \; \boldsymbol{\Xi} = \left\{ \xi_{pq}^{l_t} \right\}_{p=1,q=1,l_t=1}^{P,Q,L_t}$ , where  $\xi_{pq}^{l_t} = SINR_{pq}^{l_t} \left( \boldsymbol{\Psi}^r \right)$ , thus converting the optimization problem (P3) to the optimization problem (P7) as

$$P7: \max_{\boldsymbol{\Psi}^r, U^r, \boldsymbol{\Xi}} \quad U^r, \tag{14a}$$

s.t. 
$$0 \le Tr\left(\boldsymbol{X}_{q,n_r}\boldsymbol{\varPsi}^r\right) \le 1, \forall q, \forall n_r,$$
 (14b)

$$\boldsymbol{\varPsi}^r \succeq 0, \tag{14c}$$

$$Tr\left(\boldsymbol{D}^{r}\boldsymbol{\varPsi}^{r}\right)=1,\tag{14d}$$

$$\sum_{p=1}^{P} \sum_{q=1}^{Q} \frac{1}{PQ} \xi_{pq}^{l_t} \ge U^r, \forall l_t, \tag{14e}$$

$$\xi_{pq}^{l_t} Tr\left(\boldsymbol{M}_{pq}^{IN'} \boldsymbol{\Psi}^r\right) \leq Tr\left(\boldsymbol{M}_{pq}^{l_t'} \boldsymbol{\Psi}^r\right),$$

$$\forall p, \forall q, \forall l_t,$$

$$(14f)$$

where (14b) is the magnitude constraint, (14c) is the constraint after positive semidefinite relaxation (SDR), and

(14d) represents  $s^2=1$ , where  $\boldsymbol{D}^r$  is a square matrix of dimensions  $QN_r+1$  with all zeros except for the last element, which is 1. The constraints (14e) and (14f) are transformed from two substitute variables, where  $\boldsymbol{M}_{pq}^{IN'}$  and  $\boldsymbol{M}_{pq}^{l'}$  represent the matrix  $\boldsymbol{M}_{pq}^{IN}$  and  $\boldsymbol{M}_{pq}^{lt}$  expanded by one row and one column of zeros, respectively, and  $\boldsymbol{M}_{pq}^{lt}=\sum_{i_r=1}^{I_r}\left[\left(\boldsymbol{W}_{pq}^{lt}\boldsymbol{X}_q^r\right)^H\boldsymbol{W}_{pq}^{lt}\boldsymbol{X}_q^r\right]$ , with  $\boldsymbol{W}_{pq}^{lt}=\beta_{pq}^{lt}\left(\boldsymbol{Q}_q^r\circ\boldsymbol{\Gamma}_q^r\right)^Tdiag\left(\boldsymbol{A}_{pq}^{lt}\boldsymbol{X}_p\boldsymbol{J}_{pq}^{lt}(i_r)\right),~\boldsymbol{M}_{pq}^{IN}=\sum_{l=1,l\neq l_t}^{L}\boldsymbol{M}_{pq}^l+\sum_{i_r=1}^{I_r}\left(\boldsymbol{W}_{pq}^N\boldsymbol{X}_q^r\right)^H\boldsymbol{W}_{pq}^N\boldsymbol{X}_q^r$ , with  $\boldsymbol{W}_{pq}^N=(\boldsymbol{Q}_q^r\circ\boldsymbol{\Gamma}_q^r)^Tdiag\left(\boldsymbol{N}_{pq}(i_r)\right)$ . The method for solving problem (P7) is the same as problem (P5), which is omitted here.

# C. Complexity and Convergence Analysis

The complexity of Algorithm 1 is mainly dominated by the SDP problems in (P5) and (P7), which are assumed to be solved by interior point method (IPM) with  $\epsilon_{IPM}$  as the convergence parameter. Suposing that Algorithm 1, (P5), and (P7) are iterated m,  $k^t$ , and  $k^r$  times respectively, the computational complexity of Algorithm 1 is  $O(mk^{t}\sqrt{PQL_{t}+PN_{t}+P+2}\log(1/\epsilon_{IPM}^{t})(PN_{t}+1)^{3.5})+$  $O\left(mk^r\sqrt{PQL_t+QN_r+2}\log\left(1/\epsilon_{IPM}^r\right)(QN_r+1)^{3.5}\right)$ . In the k-th iteration when solving (P5), due to constraint (13c),  $U^{t(k)} \geq U^{t(k-1)}$ . In each iteration,  $U^t$  is monotonically non-decreasing and has an upper bound due to the power constraint (13b), so the problem (P5) is convergent. Likewise, the problem (P7) is also convergent. When solving (P1) it is easy to introduce  $U^{r(m)} > U^{t(m)} > U^{r(m-1)} > U^{t(m-1)}$ in the m-th iteration. Therefore, the smallest  $\overline{SINR}^{l_t}$  is monotonically non-decreasing and has an upper bound due to the power constraint (13b), so the Algorithm 1 is convergent.

# V. SIMULATION RESULTS

In this section, simulation results are provided to evaluate the performance of the proposed distributed RHS radar system. The carrier frequency of the radar signal is  $f_c = 30GHz$ , the wavelength  $\lambda = 1cm$ , and the radiation power of each subarray  $P_M = 4mW$ . The element spacing of RHS is  $\lambda/3$ , and the number of feeds per subarray is K=5. We set waveguide refraction coefficient  $\nu = \sqrt{3}$  and amplitude attenuation factor a=5. Suppose that there are two targets, one clutter in the system, located at  $p_1 = [1/2, \ 2, 1]$ ,  $p_2 = [1, \ 3/2, 1]$ ,  $p_3 = [1, \ 2, \ 2]$ , with power  $\sigma_1^2 = \sigma_2^2$ ,  $\sigma_3^2$ , respectively. We set noise power  $\sigma_n^2 = 4uW$ ,  $SNR = 10\log_{10}\left(\sigma_1^2/\sigma_n^2\right) = 6dB$  and interference-to-noise ratio, i.e.  $INR = 10\log_{10}\left(\sigma_3^2/\sigma_n^2\right) = 6dB$ . To evaluate the performance of the proposed scheme, we also provide a comparison between it and the distributed phased-MIMO scheme with the equivalent power consumption and hardware cost.

Fig. 2(a) shows SINR versus hardware cost of the proposed scheme (RHS) and the distributed phased-MIMO scheme (phased array) with  $\delta=6,8,10$ . For simplicity, the hardware cost of a phased array antenna is normalized to 10. Therefore, the hardware cost of an RHS element is  $10/\delta$ . Hardware cost denotes  $N_{sum}*10/\delta$ . We set P=Q=2, and the hardware cost of the system is increased by increasing the number of

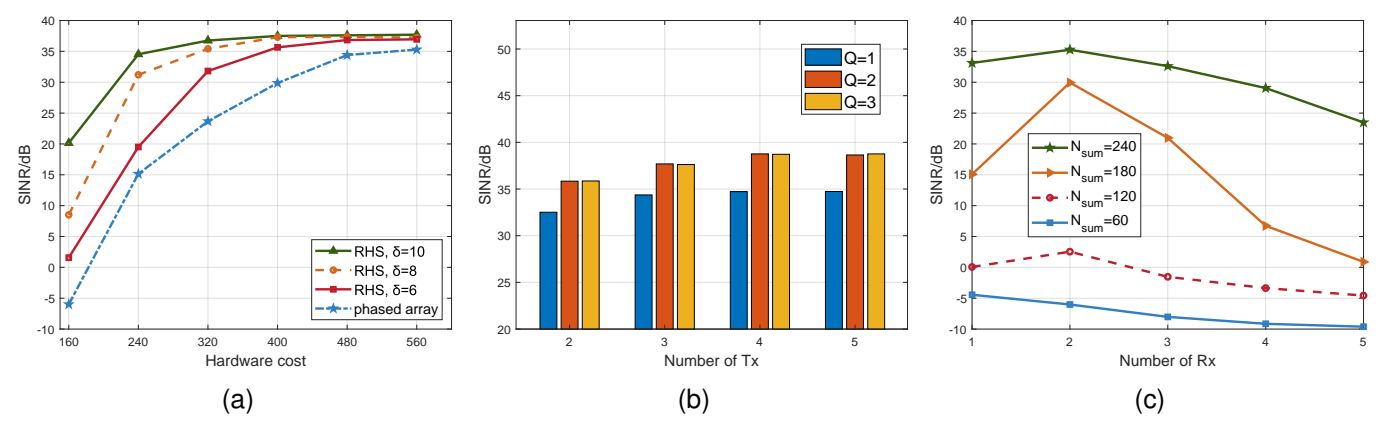


Fig. 2. (a) SINR versus hardware cost; (b) SINR versus number of Tx; (c) SINR versus number of Rx.

elements per subarray. We observe that compared with the distributed phased-MIMO scheme under the equivalent power consumption and hardware cost, the SINR of the proposed RHS scheme exceeds at least 4.98dB on average, indicating that the proposed system achieves significantly better multitarget detection performance.

Fig. 2(b) depicts SINR versus number of Tx, i.e. P, with different number of Rx, i.e. Q. We set the number of elements per subarray  $N_t = N_r = 80$ . It is shown that, given Q, SINR increases with the number of Tx and reaches saturation at P = 4. Similarly, given P, SINR increases with the number of Rx and reaches saturation at Q = 2. This indicates that increasing the number of Tx or the number of Rx brings spatial diversity gain, which improves the performance of multi-target detection until saturation.

Fig. 2(c) illustrates SINR versus number of Rx with different  $N_{sum}$  of the system. The number of Tx P is set to 2. It can be seen that when  $N_{sum}=60$ , SINR decreases as the number of Rx increases, which indicates that the spatial diversity gain brought by increasing Rx is not enough to compensate for the reduced signal coherence processing gain. When  $N_{sum}=120,180,240$ , SINR increases first and then decreases as the number of Rx increases, and reaches a peak at Q=2. It suggests that given the system hardware resources, there is an optimal system configuration, which achieves the optimal allocation between the signal coherent processing gain and the spatial diversity gain, so as to maximize the probability of multi-target detection.

## VI. CONCLUSION

In this letter, we have developed RHS-aided distributed MIMO radar systems for multi-target detection. In order to optimize the performance of the system, for each target, We have maximized the minimum SINR average of all radar subsystems, and have designed an optimization scheme for joint transceiver subarrays beamforming. Through the simulation results, we can draw the following conclusions: 1) Compared to distributed phased-MIMO radar systems with equivalent power consumption and hardware cost, the proposed scheme achieves superior multi-target detection performance. 2) Increasing the number of elements per subarray and the number of subarrays

improves the performance of the system by enhancing the signal coherence processing gain and spatial diversity gain, respectively, and achieves saturation. 3) With fixed hardware resources, optimal system performance can be attained by appropriately allocating coherent processing gain and spatial diversity gain through the configuration of array elements.

#### REFERENCES

- [1] A. M. Haimovich, R. S. Blum, and L. J. Cimini, "Mimo radar with widely separated antennas," *IEEE Signal Process. Mag.*, vol. 25, no. 1, pp. 116–129, Dec. 2007.
- [2] C. Qi, J. Xie, H. Zhang, Z. Ding, and X. Yang, "Optimal configuration of array elements for hybrid distributed pa-mimo radar system based on target detection," *Remote Sens.*, vol. 14, no. 17, p. 4129, Aug. 2022.
- [3] M. A. ElMossallamy, H. Zhang, L. Song, K. G. Seddik, Z. Han, and G. Y. Li, "Reconfigurable intelligent surfaces for wireless communications: Principles, challenges, and opportunities," *IEEE Trans. Cogn. Commun. Netw.*, vol. 6, no. 3, pp. 990–1002, Sept. 2020.
- [4] S. Zhang, H. Zhang, B. Di, Y. Tan, M. Di Renzo, Z. Han, H. V. Poor, and L. Song, "Intelligent omni-surfaces: Ubiquitous wireless transmission by reflective-refractive metasurfaces," *IEEE Trans. Wireless Commun.*, vol. 21, no. 1, pp. 219–233, Jan. 2021.
- [5] R. Deng, B. Di, H. Zhang, and L. Song, "Hdma: Holographic-pattern division multiple access," *IEEE J. Sel. Areas Commun.*, vol. 40, no. 4, pp. 1317–1332, Jan. 2022.
- [6] P. Staff, "Holographic beamforming and phased arrays," Pivotal Commware, Inc., Kirkland, WA, USA, pp. 68–73, 2019.
- [7] Q. Li, M. El-Hajjar, Y. Sun, and L. Hanzo, "Performance analysis of reconfigurable holographic surfaces in the near-field scenario of cell-free networks under hardware impairments," *IEEE Trans. Wireless Commun.*, Sept. 2024.
- [8] Q. Li, M. El-Hajjar, C. Xu, J. An, C. Yuen, and L. Hanzo, "Stacked intelligent metasurfaces for holographic mimo aided cell-free networks," *IEEE Trans. Commun.*, Nov. 2024.
- [9] H. Zhang, H. Zhang, B. Di, Z. Han, and L. Song, "Holographic radar: Optimal beamformer design for detection accuracy maximization," in 2023 IEEE Radar Conference (RadarConf23), San Antonio, TX, USA, May 2023, pp. 1–6.
- [10] X. Zhang, H. Zhang, R. Deng, L. Liu, and B. Di, "Multi-target detection for reconfigurable holographic surfaces enabled radar," in GLOBECOM 2023, Kuala Lumpur, MYS, Dec. 2023, pp. 6634–6639.
- [11] R. Deng, B. Di, H. Zhang, Y. Tan, and L. Song, "Reconfigurable holographic surface-enabled multi-user wireless communications: Amplitude-controlled holographic beamforming," *IEEE Trans. Wireless Commun.*, vol. 21, no. 8, pp. 6003–6017, Jan. 2022.
- [12] X. Yu, K. Alhujaili, G. Cui, and V. Monga, "Mimo radar waveform design in the presence of multiple targets and practical constraints," *IEEE Trans. Signal Process.*, vol. 68, pp. 1974–1989, Mar. 2020.
- [13] Z.-q. Luo, W.-k. Ma, A. M.-c. So, Y. Ye, and S. Zhang, "Semidefinite relaxation of quadratic optimization problems," *IEEE Signal Process. Mag.*, vol. 27, no. 3, pp. 20–34, Apr. 2010.